Geotech Geol Eng
https://doi.org/10.1007/s10706-018-0598-4

ORIGINAL PAPER

Effectiveness of Lime Treatment of Coarse Soils Against Internal Erosion

R. Elandaloussi · A. Bennabi · J. C. Dupla · J. Canou · A. Benamar · P. Gotteland

Received: 12 June 2017 / Accepted: 4 June 2018

Abstract The construction of embankments and other earth hydraulic structures using coarse soils requires assessing their potential for internal erosion by suffusion, defined as detachment and transport of fine particles through the matrix constrictions under internal flow. For potentially erodible coarse soils containing a certain amount of clays, a possible remedial solution is the lime treatment which is studied in this work in an experimental program consisting in: erosion test, crumb test, unconfined compression test and microstructure characterization tests (SEM, mercury intrusion porosity). The experiments were carried out on a reconstituted soil owing similar characteristics to natural coarse soils. The treatment reported in this study is carried out using a minimum lime content of only 1%, which can be achieved in situ in a cost-effective manner. Comparisons of results on treated and untreated soils showed that the lime treatment is effective after only 24 h of treatment. The suffusion is stopped, the agglomeration of the particles generated by the treatment seems to be maintained after samples immersion and the unconfined compressive strength (UCS) is improved. The microstructure observations of the fine part of the soil (particles smaller than 1 mm) showed the appearance of agglomerates generating an increase of the pore volume.

Keywords Erosion · Lime treatment · Coarse soil · Crumb test · Compression test · Scanning electron microscopy · Mercury intrusion porosimetry

1 Introduction

The construction of hydraulic structures requires the use of stable soil against internal erosion. In many parts of France, where the construction of these structures is necessary, local soil deposits, including coarse soils containing a small percentage of clay, are not suitable. Due to their poor characteristics, these soils are stoked and substituted by other soils transported from other regions, which is far from being satisfactory in economic terms. One possible solution, commonly used in geotechnical engineering for other applications, is to enhance the characteristics of these

R. Elandaloussi (✉) · J. C. Dupla · J. Canou
Ecole des Ponts ParisTech, UR Navier, CERMES, 6 et 8 avenue Blaise Pascal, Cité Descartes, Champs-sur-Marne, 77455 Marne-La-Vallée Cedex 2, France
e-mail: radja.elandaloussi@enpc.fr

A. Bennabi
Université Paris-Est, ESTP Paris , Institut de Recherche en Constructibilité (IRC), 94230 Paris, France

A. Benamar
Normandie Université, UNIVHAVRE, CNRS, LOMC, 76600 Le Havre, France

P. Gotteland
Fédération Nationale des Travaux Publics, Paris, France

Published online: 09 June 2018

coarse soils against suffusion by a lime treatment. The expected improvements will allow to reduce the costs and delays of the construction site and also to be a part of a sustainable development approach.

Soil stabilization with lime is a technique commonly used in earthworks since the middle of the past century. In the literature, this treatment technique is related only to fine grained soils like silty soils (Cuisinier et al. 2011; Makki-Szymkiewicz et al. 2015; Le Runigo et al. 2011), or clayey soils (Lasledj 2009; Al-Mukhtar et al. 2010; Lemaire et al. 2013; Tran et al. 2014). However, the use of lime treated soils in hydraulic context is less known, at least in Europe. In the United States and Australia, the authorities restore and reinforce some hydraulic earthworks since the 1970's (Howard and Bara 1978; Perry 1977; ANCOLD 1978), the Friant-Kern irrigation canal in California was probably the best tesmonial for the relevance and efficiency of soil lime treatment for hydraulic use (Charles et al. 2012). In 2005, in France, the Lhoist Group has launched a series of experimental programs on a dike constructed of lime treated silty soil. Some tests have been carried out on site and some others in the laboratory. The results are presented in the work of Haghighi (2012). With the hole erosion test, sudden fracturing occurs at high pressure.

The properties of soil–lime mixtures depend on the quality of added lime, the chemical and mineralogical composition of the soil (Boardman et al. 2001) and the compaction conditions (Petry and Berger 2006; Le Runigo 2008). Several works on lime treatment showed that there are two distinct processes that take place when lime is added to wet soil. First an immediate change is observed, which is related to a modification of the soil structure. According to Rogers and Glendinning (1996), Al-Mukhtar et al. (2012) and Tran et al. (2014) this is related to a cation exchange process where the calcium ions (Ca^{2+}) migrate from hydrated lime to the surface of the clay particles and displace water and other ions. This process results in soil "flocculation and agglomeration" and lasts a few hours depending on the characteristics of the clay mineral involved. These reactions modify the clay texture, give thicker particles, reduce plasticity and increase the soil strength (Basma and Tuncer 1991; Khattab 2002; Charles et al. 2012).The soil becomes friable and granular after this phase (Tran et al. 2014) which impacts the soil microstructure, as for example in terms of its pore size distribution (Osula 1996). When the quicklime is used, another short-term process corresponds to its hydration which is an exothermic reaction occurring immediately between quicklime and water to form hydrated lime. The second phase corresponds to a long-term process. It is the stabilization phase due to the pozzolanic reaction which occurs more slowly over a long period of time and depends on temperature, soil chemistry and mineralogy (Hunter 1988; Wild et al. 1993). During this process, the high pH value in soil causes silica and alumina dissolution and their combination with calcium, producing cementitious compounds, calcium silicate hydrates (CSH) and calcium aluminate hydrates (CAH) (Choquette et al. 1987; Locat et al. 1996). These processes contribute, in particular, to improve the mechanical properties of the soil. This study consists in checking the effectiveness of the lime treatment of a particular coarse soil in order to ensure its stability against internal erosion by suffusion, and in identifying the main processes involved.

The aim of this paper is: (1) to investigate whether the lime treatment is able to improve the resistance to erosion of a coarse soil containing a low proportion of clay; (2) to study the evolution of the soil properties at one day of curing and (3) to address the impact of different hydraulic conditions, i.e. water content, saturation rate and water circulation on the mechanical performance and resistance against erosion.

In order to understand the improvement of the characteristics of a coarse soil initially prone to suffusion and treated with lime, different experiments were carried out in this study: erosion test, crumb test, unconfined compression test and microstructure characterization tests such as scanning electron microscopy (SEM) and mercury intrusion porosity (MIP).

2 Materials and Methods

2.1 Materials Properties

2.1.1 Reconstituted Soil

In order to investigate a soil from a river embankment located in the center of France close to Lyon region, a similar reference reconstituted coarse soil is created in the laboratory which is very close to the natural soil, because this reconstitution will ensure a good

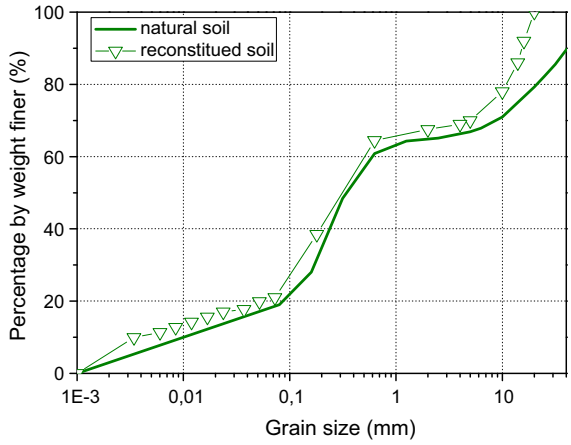

Fig. 1 Grain size distribution of tested soils

Fig. 2 Gravel washed and fractionated

Table 1 Characteristics of used sand

Sable	d_{50} (μm)	Cu	Size distribution
Hostun HN2/4	2849	1.4	Uniform
Hostun HN0.4/0.8	596	1.5	Uniform
Hostun: HN31	314	1.3	Uniform
Hostun: HN34	211	1.6	Uniform
Hostun HN38	113	2.3	Uniform

repeatability of the tests and enables easily to control the proportion of fines within the coarse matrix. The field soil is a gravelly sandy soil with fines classed B according to French standards AFNOR (1992) NF P 11-300. This soil is essentially characterized by a spread but discontinuous grading curve as shown in Fig. 1.

The soil reconstitution in the laboratory is performed by mixing gravels, sand and fines with well-defined proportions. The fine part of particles consists of kaolinite and crushed sand (sand particles of size less than 80 μm). Rounded gravels have been split into fractions 31.5/20, 20/16, 16/14, 14/10, 10/6.3, 6.3/4 (Fig. 2) as recommended by the French standard AFNOR (1993) NF P 98-230-3.

The used sand is Hostun sand which was separated into several fractions namely HN2/4, HN0.4/0.8, HN31, HN34 and HN38 (Table 1) , The SEM views of two fractions of Hostun sand are presented in Fig. 3.

The fine part (d $<$ 80 μm) consists of 40% kaolinite clay (K) and 60% crushed sand (C4). The characteristics of the obtained mixture are shown in Table 2.

2.1.2 Lime

The lime used in this study is quicklime, commercially named Proviacal ST and provided by Lhoist Company. The characteristics of this lime are indicated in Table 3. An X-ray diffraction analysis showed the presence of calcite (Fig. 4) indicating that this lime is a partially carbonated lime.

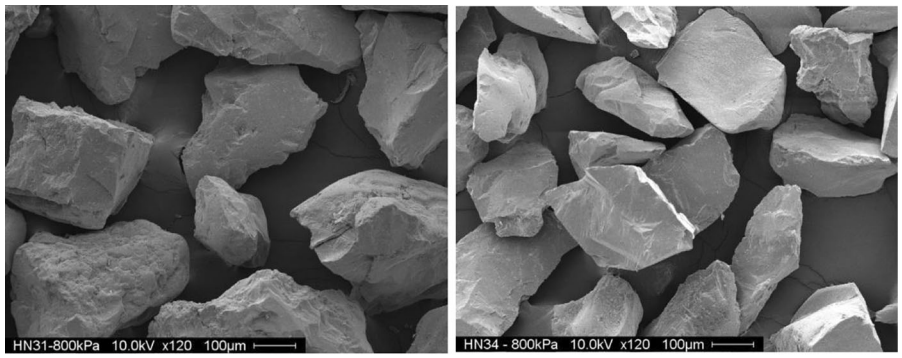

Fig. 3 SEM views of: **a** Hostun sand HN31, **b** Hostun sand HN34 (Feia et al. 2015)

Table 2 Characteristics of the fine soils used

	Characteristics	C4–K
Atterberg limits	Liquid limit ω_l (%)	33
	Plastic limit ω_p (%)	21
	Plasticity index I_P	12
Grain size distribution	< 80 µm	65%
	< 2 µm	30%
	D_{60} (µm)	60

Table 3 Lime characteristics

Characteristics	Value at 20 °C
Bulk density (t/m^3)	0.7–1.3
pH on saturated solution	12.3

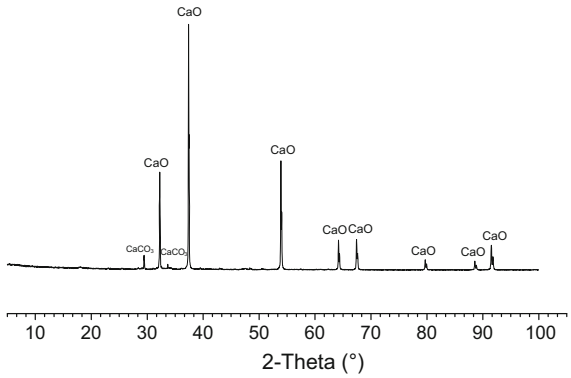

Fig. 4 X-ray diffraction for lime

2.2 Preparation and Compaction Procedure

In order to prepare the untreated soil sample, with a compaction at 95% of the maximum Standard Proctor Density (SPD) on the wet side (13% water content) (Fig. 5), the different required proportions of sands, kaolinite and water are mixed in a blender for 3 min at a constant speed around 70 rpm. Then, the gravels are added and mixed with the other materials by hand. Once the sample reconstitution is completed, it is kept in airtight bags for 24 h for maturation before compaction in test column.

Lime treated soil is prepared similarly to the untreated soil except few differences. After 24 h storage, the mixture "sand-kaolinite-water" is mixed again by adding a given quantity of lime. Then the proportion of gravels is added to the previously set for a dry density corresponding to 95% of the maximum SPD (Fig. 5). After 3 min of mixing with a speed of 60 rpm the mixture is kept in airtight bags for one hour curing before compaction.

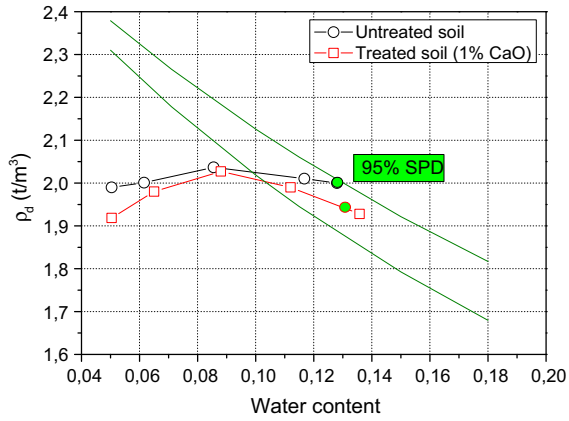

Fig. 5 Modified proctor curve

3 Experimental Devices

3.1 Erosion Set-Up

The developed set-up consists of a suffusion column with an automated hydraulic loading device, an effluent collection system, a data acquisition system and a measurement system allowing to follow the temporal evolution of pore pressure throughout the column, the effluent turbidity, the flow rate and the mass of eroded particles. Figure 6 shows a schematic view of the erosion set-up. The evolution of pore pressure along the column is measured using six sensors (C1, C2, C3, C4, C5, C6) installed at different points.

The suffusion column is a Plexiglas tube of 250 mm diameter and 600 mm height, which allows a visual inspection during experiments. In this study the height of the specimen is 160 mm along which only three pressure sensors are placed at the top of the specimen (Fig. 6). The column is arranged vertically and is supplied by a water tank for an upward flow. It should be noted that the top of the column is not blocked by a watertight cover. An overload of 1.6 kPa (half of the stress due to the weight of the sample) is

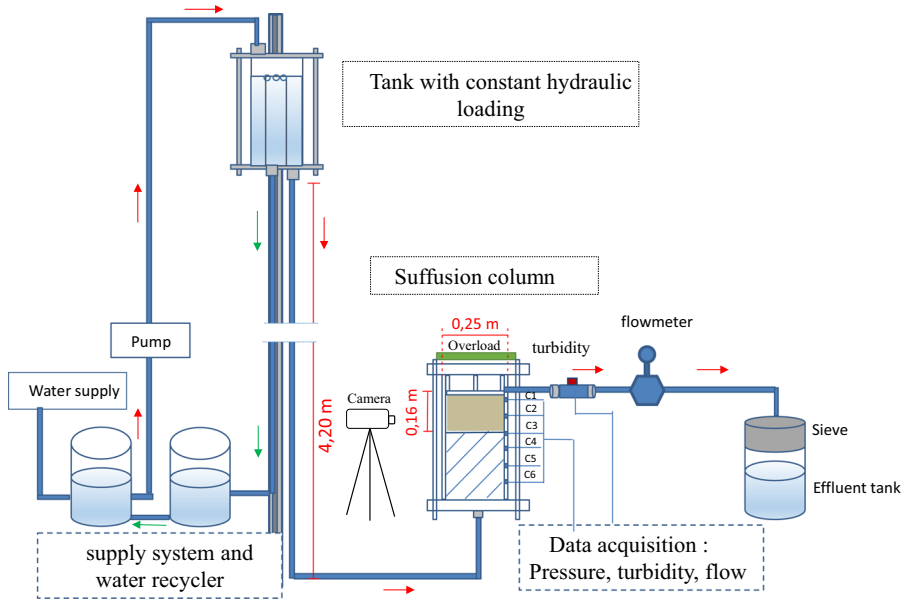

Fig. 6 Functional diagram of the internal erosion testing device

applied to prevent the sample from moving. The tank position depends on the target hydraulic gradient, knowing that this latter represents the piezometric head drop per unit length. The effluent is collected in order to determine the total mass of eroded particles.

The soil sample was deposited within the suffusion column in two layers of 80 mm each which were compacted using the normal Proctor hammer at the target density of 95% SPD. The specimen rests on a lower mesh screen (80 µm opening size), supported by a metal grid, placed itself on a gravel layer of approximately 10 mm in diameter. The mesh screen placed between the grid and the soil sample allows avoiding a loss of fine particles (Fig. 7). Once the reconstituted sample is set up and the tubing circuit is saturated, the test circuit is closed. The saturation of the sample is started by applying a low hydraulic gradient of approximately 1.

3.2 Experimental Setup for Modified Crumb Test

This simple test is carried out based only on visual observations for a qualitative assessment of clay dispersion. It is derived from crumb test as detailed in ASTM standard D 6572-13 (2013); some modifications were made in order to adapt it to our samples.

The complete setup consists of a 100 mm diameter and 200 mm height PVC mold for soil samples, a glass water tank of 380 × 380 mm horizontal section and 430 mm height (50 L working volume), the lighting, a grid used to lift the sample and a camera (Fig. 8).

The soil sample was deposited in the PVC tube in one layer of 200 mm each which are compacted using the normal Proctor hammer at the target density of 95% SPD.

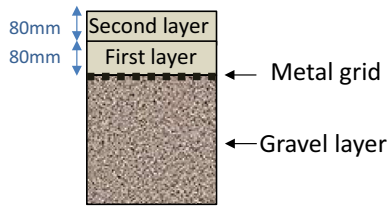

Fig. 7 Descriptive diagram of the sample in the column

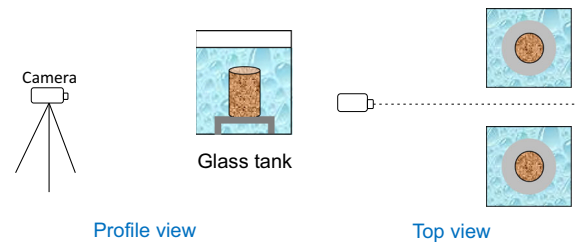

Fig. 8 Functional diagram of crumb test device

3.3 Unconfined Compression Test

Unconfined compression tests were carried out according to AFNOR (1997) NF 94-077. The soil specimens prepared for the unconfined compression tests are 100 mm diameter by 200 mm height. The used device is an MTS press with a moving speed of 1 mm/min. This loading speed was previously used by Maubec (2010) for the evaluation of the unconfined compression strength of clay soils. These mechanical tests are carried out on samples to study the influence of the lime treatment on the mechanical behavior after compaction and on samples after the crumb test if they do not collapse after 6 days of immersion.

3.4 Microstructure Characterization Tests

The microstructure of treated and untreated soil samples were characterized by means of several techniques: mercury intrusion porosimetry (MIP), the grain size analysis (Malverne multisizer) for the size fraction lower than 1 mm and SEM observations.

The microstructure characterizations by MIP had to be performed on dry samples prepared using freeze-drying method. The soil samples were immersed in liquid nitrogen for freezing and placed in a freeze dryer for 24 h of sublimation. Quick freezing minimizes microstructural change due to water departure (Delage and Pellerin 1984). At the first, the grain size analysis provided grain size distribution of the soil's fine fraction. Subsequently, micro-level observations were recorded on fresh samples using SEM. And finally, the mercury intrusion porosimetry (MIP) was selected to investigate the fabric of the samples because this method allows the measurement of a wide pore-size range, from a few nanometers up to several tens of micrometers, and the identification of different soil pore classes.

4 Results and Discussion

4.1 Erosion Tests

In this section, we present the detailed results of two tests performed with untreated soil and with 1% lime treated soil for 24 h of curing time. A comparison was performed with other curing duration (7, 28, 90 and 365 days) in the aim to detect the best/optimal curing time for improvement of soil characteristics against suffusion.

4.1.1 Untreated Soil

In this part, we will identify and explain the initiation and development of internal erosion processes observed in the case of untreated soil subjected to an upward unidirectional flow.

Figure 9 shows the evolution of pressure on the three sensors C_1, C_2 and C_3. There is a general decrease of pressure on the three sensors only 5 min after applying the mean gradient i = 3. This decrease is more pronounced at the sensor C_3 located at the bottom of the sample. The pressure at the sensor C_3 decreases from 5.3 to 1.7 kPa. This pressure drops at the upstream of the soil sample may be explained by a

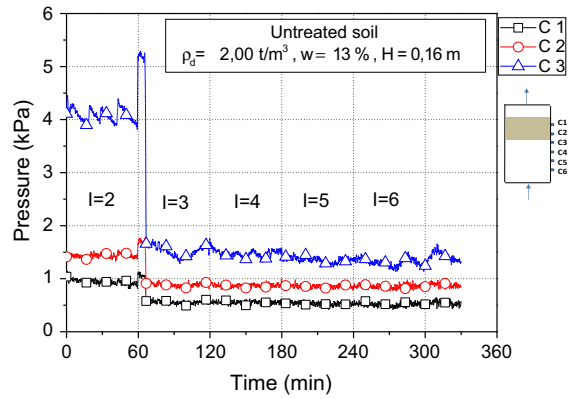

Fig. 9 Evolution of pressures during the loading phase for the untreated soil

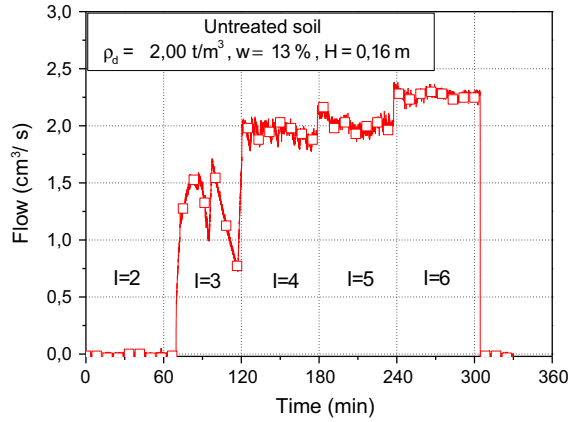

Fig. 10 Evolution of flow during the loading phase for the untreated soil

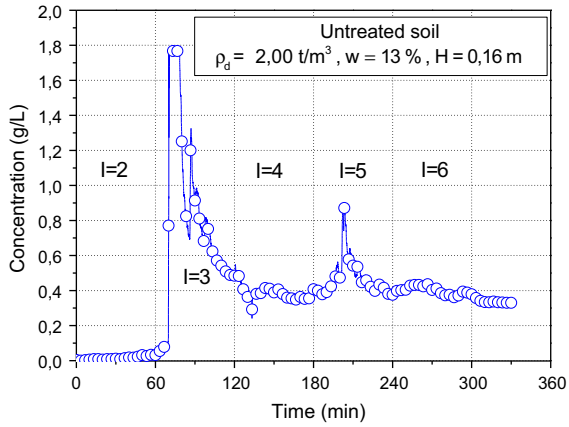

Fig. 11 Evolution of concentration during the loading phase for the untreated soil

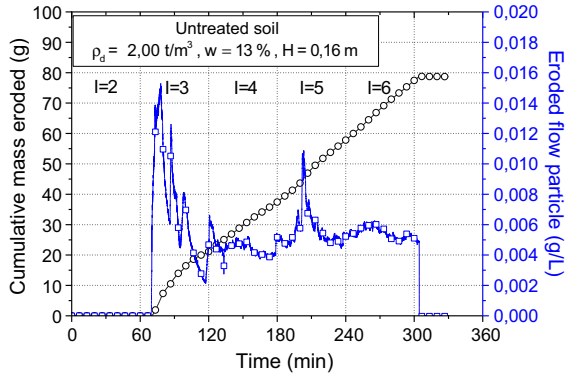

Fig. 12 Evolution of cumulative eroded mass and eroded particles flow during the loading phase for the untreated soil

detachment and a massive erosion of particles allowing the free flow of the water, whose rate increases immediately from zero to 1.5 cm^3/s (see Fig. 10).

Figure 10 shows the evolution of the flow rate during the loading phase. During the application of the gradient i = 3, there was a fast increase of the flow rate, probably due to the moving of particles, reaching a value close to 1.5 cm^3/s. Then, there is a flow rate fluctuation, due to the restructuration of fine particles into the specimen matrix. At the gradient i = 4, the flow rate stabilizes around 1.9 cm^3/s and at the gradient i = 5 there is a slight decline of the flow rate at the first 30 min before it stabilizes around 2 cm^3/s.

Figure 11 displays the evolution of effluent concentration (obtained from turbidity measurements correlated to fines concentration), and indicates a first peak of solid flow 5 min after applying the gradient i = 3, confirming the particles migration hypothesis advanced earlier after the fall of pressure. This proves that there is a restructuring of the particles within the granular matrix by generating clogging. Another peak was observed 30 min after the start of the application of the gradient i = 5, and was due to the expansion of the clogging phenomenon after plugging. This process results in the flow decrease observed on Fig. 10.

Figure 12 shows the evolution of the erosion rate from the concentration of the effluent and the flow rate, and also gives the evolution of the cumulated mass eroded during the test. The initiation to the suffusion (at the gradient i = 3) is coupled with a rapid increase of the effluent concentration (and, therefore, of eroded cumulative mass). At the end of the load at a gradient i = 3, the mass of eroded particles is approximately 18 g (22.5% of the total eroded mass). The rapid increase of the cumulative mass of eroded particles at the beginning of the test reflects the important contribution of the peak concentration to the total mass mobilized.

From the gradient i = 4, a slower and quasi-linear increase is observed for the cumulative eroded mass, indicating a low contribution of the concentration curve. The curve of cumulative mass eroded in Fig. 12 is composed of two parts. The first one (until 120 min) corresponds to the massive suffusion for i = 3, then followed by a steeper slope part representing the moderate suffusion kinetics in the following gradients.

At the end of the test, the cumulative weight calculated from measurements of turbidity and flow rate indicates a value close to 79 g. In order to identify

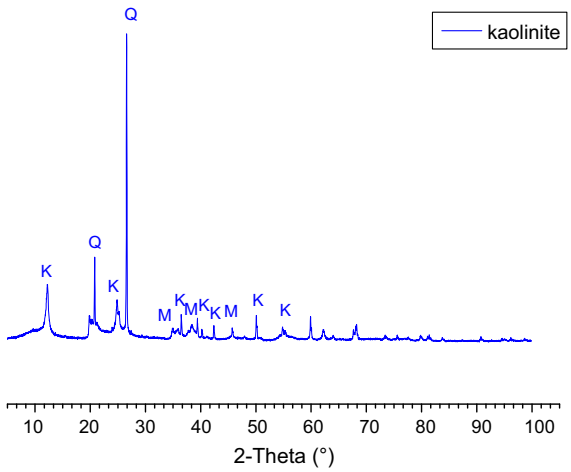

Fig. 13 X-ray diffraction of the eroded particle

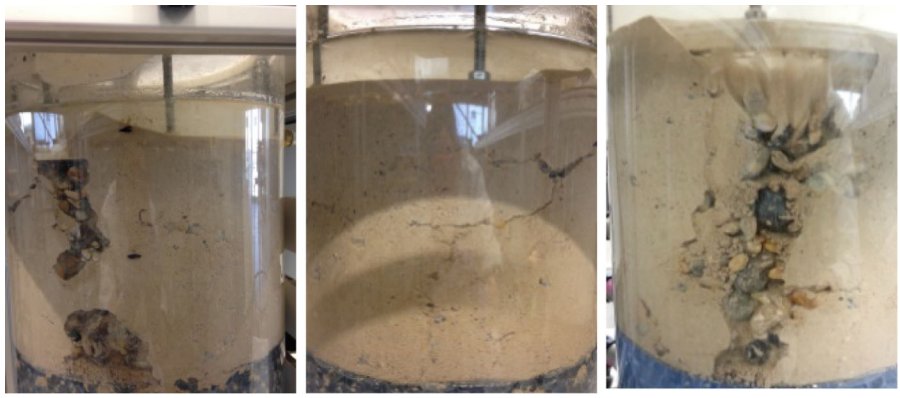

Fig. 14 Pictures of the sample taken at the end of the test

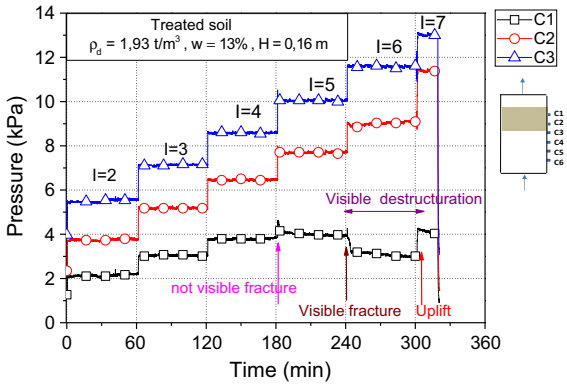

Fig. 15 Evolution of pressures during the loading phase

the nature of eroded particles, X ray diffraction analysis was carried out and showed that the eroded particles are kaolinite (Fig. 13) without any sand particles. In fact, the obtained spectrum is identical to the one of the original kaolinite used in this study.

Pictures of Fig. 14 illustrate the state of the specimen before stopping the flow at the end of the application of the gradient i = 6, one can observe a massive departure of the fines on the different sides on the column.

4.1.2 Lime Treated Soil

The hydraulic pressure within the specimen is an indicator of the effectiveness of the lime treatment which is expected to limit the soil erosion. The pressure variations recorded in the three sensors are presented in Fig. 15. Six levels of hydraulic gradient (from 2 to 7) have been applied to the sample. The first hydraulic gradient which represents the saturation step is not shown on the graph. A pressure drop is observed at the sensor C1 (top of the sample) during the application of the gradient i = 5. This is due to the beginning of the soil fracturing, which is not yet visible, but creates a preferential pathway for water pressure release.

At the gradient i = 6, small fractures develop in the sample, which are progressively enlarged until a part of the soil is lifted, creating a water pocket.

It should be noted that the first cracks, visible to the naked eye, always appear at the top (Fig. 16b). This can be explained by a downstream clogging (the particles are carried downstream where they are accumulated) causing a sudden drop pressure in the cracks area.

Through time, the cracks disappear when the pressure in the sample is stabilized; these cracks are replaced by other cracks which appear in the lower part of the sample. They open and close during the destructuring of the sample until the occurrence of a large crack through the entire cross section of the sample. This large crack expands creating a water pocket and so the phenomenon progresses from the beginning of loading until the uplifting of a portion of the sample (Fig. 16c). Figure 17 illustrates the evolution of the erosion phenomenon from the beginning of the loading up to the lifting of a part of the sample.

This division of the soil is the result of the exceeding of the total vertical stress that the soil can withstand due to the development of sufficiently high excess pore pressure in this zone situated under a layer which has become “almost” impermeable, as a result

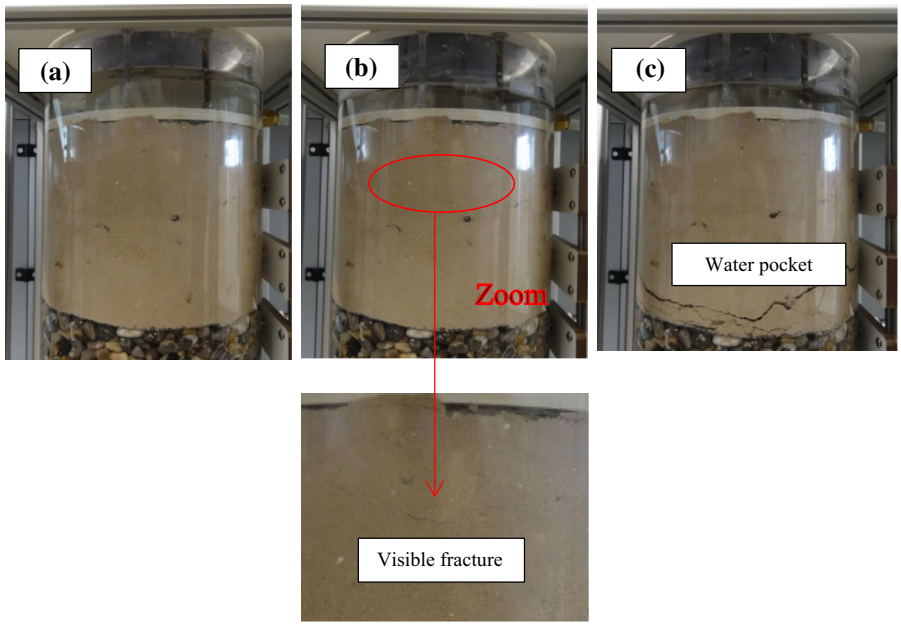

Fig. 16 Evolution of fracturing during erosion test for the treated soil

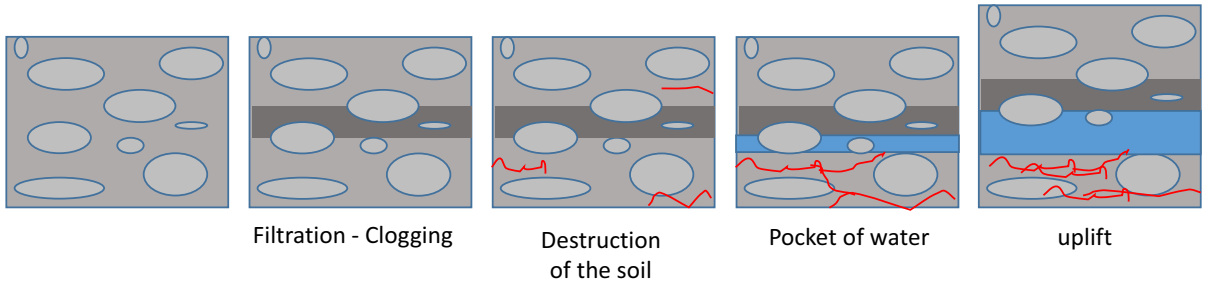

Fig. 17 Illustration of hydraulic fracturing evolution through the sample during the erosion test for treated soil

of clogging. The effective vertical stress has been reduced to zero leading to the appearance of fine fractures and consequently the appearance of a water pocket, then a progressive uplift of the soil surface and finally the total failure of the soil sample. An assessment of the local stresses state is needed for a better understanding of the triggering conditions of this phenomenon.

The lateral friction is assumed to be zero since the wall of the Plexiglas column is supposed to be perfectly smooth. Figure 18 shows the stresses applied to the base of the sample as well as the theoretical fracturing pressure.

At the bottom of the sample, theoretical fracturing pressure resulting from the stress balance sheet is 5.3 kPa (taking into account the stress due to the

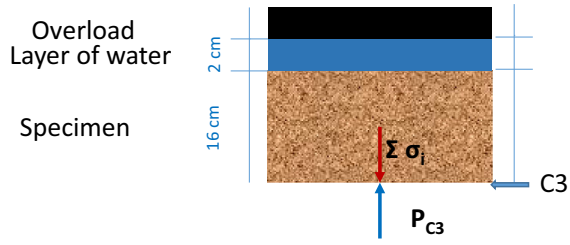

Fig. 18 Diagram expressing stresses assessments

weight of the sample, 20 mm layer of water and the stress due to the overload, see Fig. 18). However, the measured fracturing pressure recorded on the pressure sensor C3 (10 kPa) is much higher, about twice the theoretical fracture pressure. This increase can be

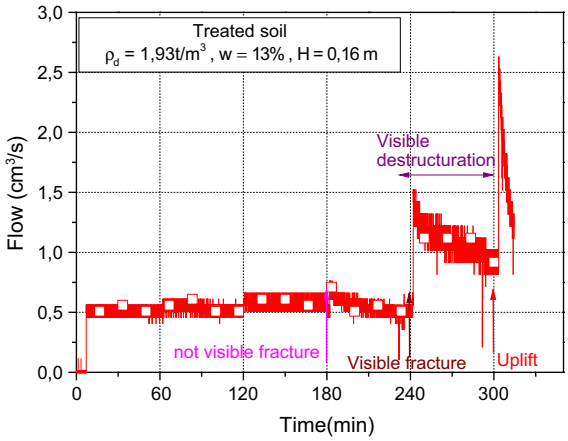

Fig. 19 Evolution of flow during the loading phase for the treated soil

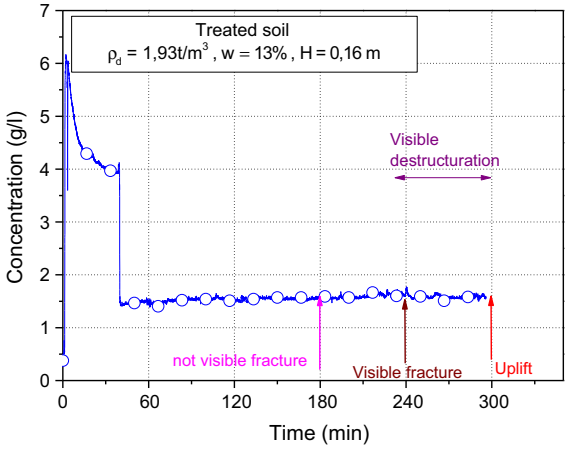

Fig. 20 Evolution of concentration during the loading phase for the treated soil

explained by the immediate effect brought by the lime treatment.

In Fig. 19, the flow rate is practically constant at the first three loading stages (i = 1, 2, 3). Then, when applying the gradient i = 5, the flow rate decreases from 0.7 to 0.5 cm^3/s, at the end of this stage. This can be explained by the hypothesis advanced above concerning the filtration and clogging of eroded particles in the sample. At the gradient i = 6, a sudden increase of flow rate reaching 1.5 cm^3/s is observed when the first fractures occur. Then the flow rate decreases progressively until the last gradient i = 7 is applied, where the formation of the water pocket occurs. Therefore, the maximum recorded flow rate reaches 2.7 cm^3/s.

As regard to particles erosion, Fig. 20 shows a concentration peak recorded at the beginning of loading at gradient i = 2, which can be attributed to the stagnation of water loaded with lime downstream the sample. This is confirmed by X-ray diffraction and fluorescence analysis performed on an effluent recovered at the end of this gradient i = 2 (Table 4,). In Fig. 20, for the higher loading stages, there is a quasi-constant turbidity around 1.5 g/L, which again proves that there is no particle erosion, but only lime leaching, and this was confirmed once again by X-ray diffraction analyzes, showing the same results as those presented in Fig. 21.

According to the X-ray fluorescence and X-ray diffraction analysis, one can observe the presence of carbonate lime in the form of $CaCO_3$ in the effluent (Fig. 21), with a fraction of about 96% (Table 4). This is confirmed by several studies (Bell 1996; Le Runigo 2008; Rossi et al. 1983) which showed the formation of calcite ($CaCO_3$) during lime treatment. This result comes from the carbonation reaction of the lime with the carbon dioxide of the air. According to Maubec (2010), for these treated soils, the mechanical performances are not, or weakly, improved by the presence of carbonates. This point will be more discussed in the presentation of the results of the mechanical tests.

Figure 22 shows the evolution of the erosion rate and the cumulative eroded mass. As previously reported, the evolution of the erosion rate presents the same trend as the turbidity during the first 40 min of experiment at a gradient i = 2. For higher gradients, the evolution of this curve follows the flow rate curve

Table 4 X-ray fluorescence analysis of the harvested effluent

Chemical formula	Concentration (%)	Chemical formula	Concentration (%)
$CaCO_3$	96.56	SO_3	0.26
SiO_2	1.75	K_2O	0.18
Al_2O_3	0.61	SrO	0.13
Cl	0.37	Fe_2O_3	0.09

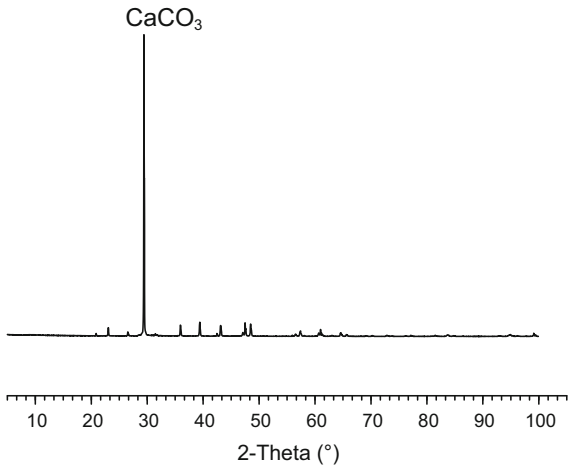

Fig. 21 X-ray diffraction analysis of the harvested effluent

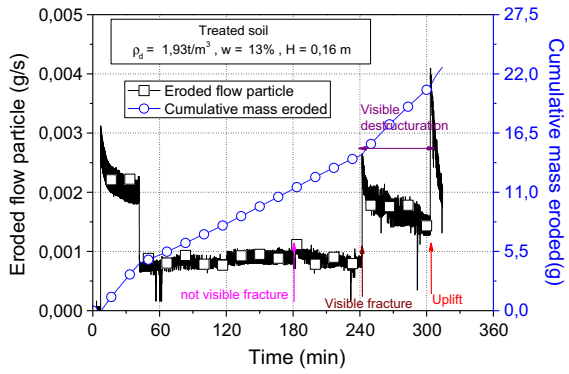

Fig. 22 Evolution of cumulative mass eroded and eroded particles flow during the loading phase for the treated sample

until the end of the test because the turbidity is quasi-constant.

The cumulative eroded mass in this case is more important than the cumulative mass of leached lime. There are three distinct slopes, the first one corresponding to the stagnation of the leached lime during the saturation which corresponds to 20% of the total mass of leached lime. The second part of the curve, with a quasi-linear slope, indicates that the quantity of leached lime is constant throughout the loading phase. During destructuration of the soil, we observe a greater increase in the mass of leached lime which is probably due to the collapse (uplift) of the soil releasing more lime trapped between the particles.

The total mass of leached lime from the sample, calculated at the end of the test, is about 24 g, which represents 16.5% of the total mass of introduced lime (Fig. 22). It is important to note that for lime-treated soil samples, the amount of lime is calculated (based on turbidity and flow rate measurements) and not measured because the water is loaded with lime and it is impossible to recover the whole quantity of leached lime even if sheets are formed as the effluent is released. This does not represent the whole leached quantity (Fig. 22). Figure 23 show the appearance of the effluent collected at the end of the test,as mentionned previously there is no erosion of particles bu only lime leaching. The color and texture of the effluent collected confirm it.

4.1.3 Repeatability of Tests

In order to verify the reliability of the obtained results, the tests presented previously were duplicated a second time (Fig. 23).

The results are synthesized in Fig. 24 in terms of the gradient of fracture and total mass of eroded particles. It should be noted that the mass of the eroded particles was measured at the same time for the two tests.

A good repeatability is observed. For the tests on untreated soil, the suffusion is triggered at gradient

Fig. 23 Visual appearance of the effluent collected at the end of the test: **a** container of the effluent harvested, **b** surface lime film, **c** recovered lime sheets

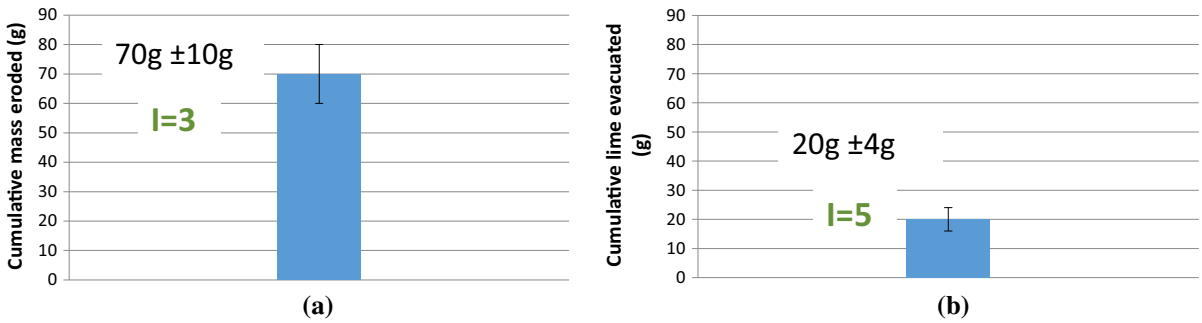

Fig. 24 Repeatability of the tests **a** untreated soil test, **b** treated soil test

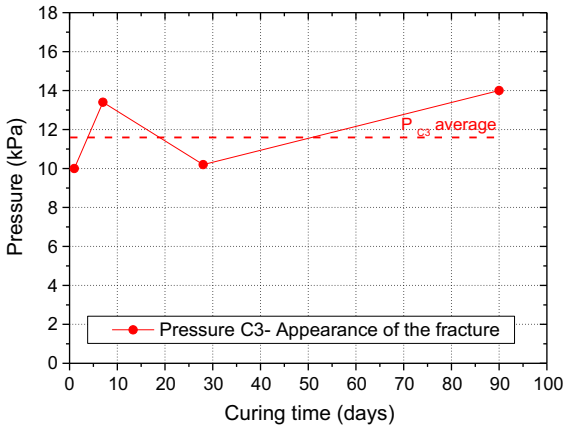

Fig. 25 Evolution of the pressure of appearance of the fracture at the sensor C3 during the curing time

i = 3 (Fig. 24a) and for tests on treated soil the beginning of breakage is at a gradient i = 5 (Fig. 24b).

4.1.4 Comparison with Long-Time Curing

In order to study the influence of the curing time on the outbreak of the fracturing process and also to determine the chemical reactions which govern this improvement of the resistance to fracturing, additional tests were carried out at longer curing times (7, 28 and 90 days).

In Fig. 25, the results show that the fracturing pressure at the sensor C3 approaches 11.8 ± 1 kPa, whatever the curing time (less or equal to 3 months). This result highlight the effectiveness of the treatment after only 24 h. It means that the first chemical reactions at short time of curing were responsible to stop the erosion phenomenon. In order to identify these reactions, the rest of this study will be focused only at this first stage of curing.

4.2 Crumb Test

The untreated soil sample collapses immediately when immersed in the water tank (Fig. 26), while the treated soil cured during 24 h with 1% lime remains substantially intact after 1 week of immersion (Fig. 27), undergoing no significant change of dimensions. This observation shows how the natural soil is susceptible to internal erosion and how lime treatment contributes to stabilize the fines against dispersion and, thus, against erosion. Also in this part, the results highlights the effectiveness of the treatment after only 24 h. It means that the first chemical reactions at short time of curing were responsible to stop the erosion phenomenon.

5 Unconfined Compression Tests Before and After Immersion in Water

The Figs. 28 and 29 show the evolution of the Unconfined Compression Strength (UCS) on untreated and treated soil without immersion and after immersion respectively. The results show a higher UCS and higher rigidity for the treated soil comparing to the untreated soil before immersion in water. After immersion, the untreated specimens almost immediately began to disintegrate. Therefore, it was not possible to determine the effect of immersion on the UCS of untreated specimens. In the case of the treated specimens, an immersion of 6 days (i.e. saturation of specimens) leads to a significant UCS decrease. This decrease was also observed by Le Runigo et al. (2011) on the Jossigny silt treated with 1% of lime.

The UCS of the treated sample is 70 kPa without immersion and approximately 12.8 kPa after immersion. The immersion of the specimen in water results in a loss of compression resistance.

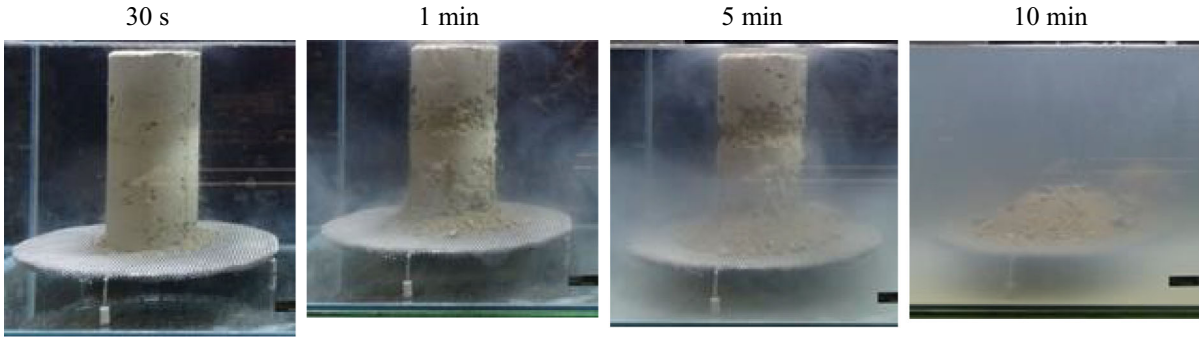

Fig. 26 Evolution of untreated soil samples during the immersion in water until collapse

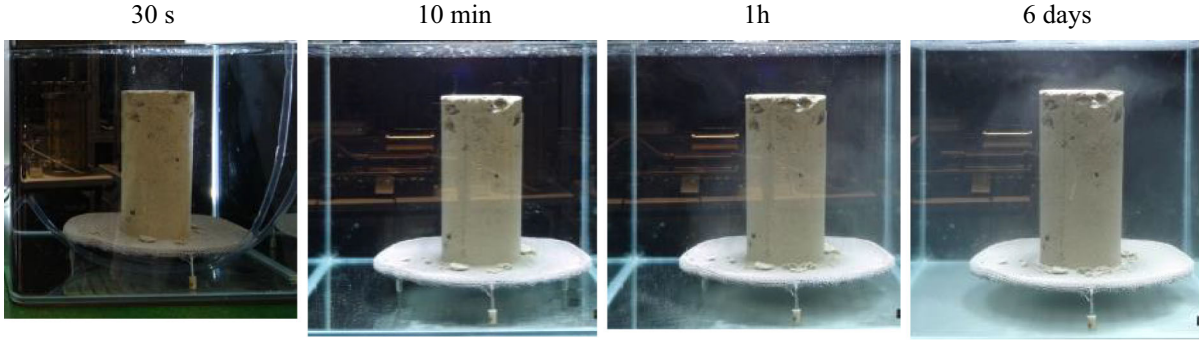

Fig. 27 Evolution of soil samples treated with 1% lime over time during the 6 days of immersion in water

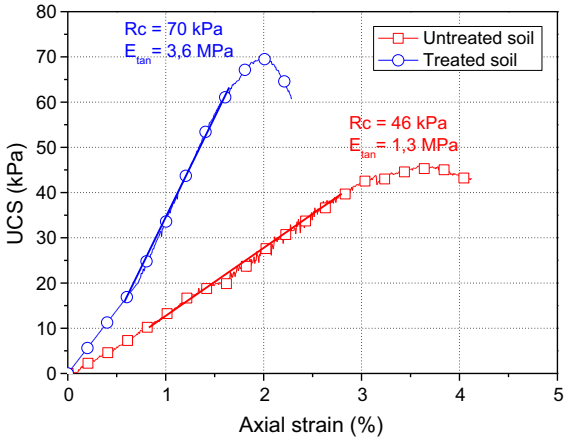

Fig. 28 Evaluation of the unconfined compression strength (UCS) for untreated and treated soil without immersion

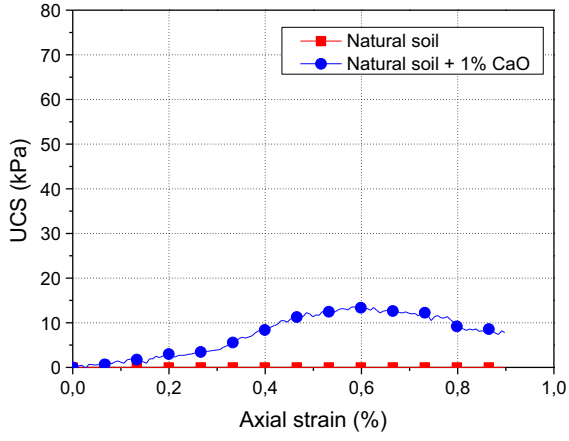

Fig. 29 Evaluation of the unconfined compression strength (UCS) for untreated and treated soil after 6 days of immersion into water

5.1 Microstructure Evolution

5.1.1 SEM Observation

Figure 30 presents the SEM observations of both untreated and treated soils. At low zoom, Fig. 30a, c show that their microstructure is totally different. For the untreated specimen, a film of clay particles is observed which covers and connects the sand grains together. A few number of inter-aggregate pores can be observed, these macrospores came from

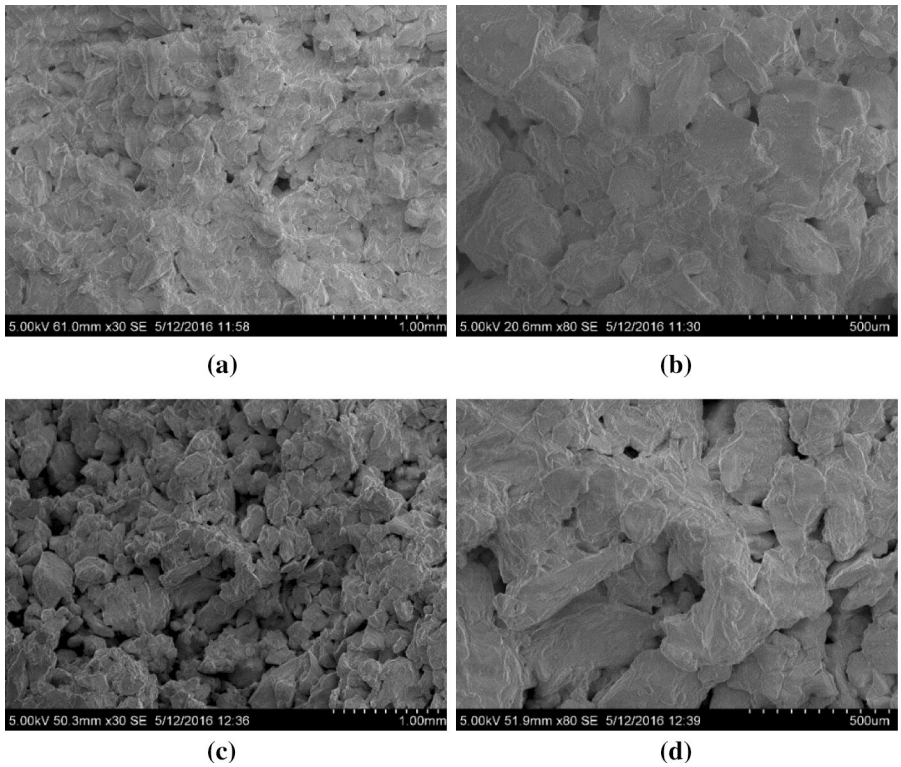

Fig. 30 SEM pictures of untreated and treated soil. **a** Untreated soil 1 mm, **b** untreated soil 500 µm, **c** treated soil, cure 24 h 1 mm, **d** treated soil, cure 24 h 500 µm

compacting (Nguyen 2015). For the lime-treated specimen, a group of agglomerates varying considerably in size is observed. At higher zoom, Fig. 30b, d, for the untreated specimen, the tightly-knit organization between clay particles and quartz grains is clearly visible which results in a few numbers of macropores. For the lime treated specimen, the structure is less tight than the structure of the untreated soil. The clay particles are in fact aggregated because of the addition of lime and form a film that coats the larger-sized quartz particles. This view of the microstructure reveals pores capable of measuring up to a few hundred microns between the agglomerates.

5.1.2 Mercury Intrusion Porosimetry (MIP)

Figure 31a shows differential mercury intrusion curves obtained for untreated and 1% lime treated soil samples at the first day of curing. On the two specimens, the pore size distribution is of a bimodal type. This type of structure is usually observed on compacted clay soils and is called "double structure" (Ahmed et al. 1974; Delage et al. 2006; Diamond 1971; Lioret et al. 2003; Stoltz et al. 2012). On untreated soil, the first mode is characterized by pore sizes ranging from 0.01 to 5 µm. From Lemaire et al. (2013) this smaller diameter class of pore may be attributed to intra-agglomerate micropores. The pore size range for the second pore family is from 20 to 120 µm, which is attributed to inter-agglomerate macropores (Fig. 31b).

After 1% lime treatment, one can observe that the pore size of the first family is also ranging from 0.01 to 5 µm; but in this case this family has much more volume. The pore size range of the second mode is from 5 to 400 µm.

The Fig. 31b shows curves of the cumulative mercury intrusion. One can observe that the total pore volume increases with lime treatment, which is compatible with SEM observations presented in Fig. 31a, b. This increase can also be attributed to the difference in the dry density between the untreated and treated soils.

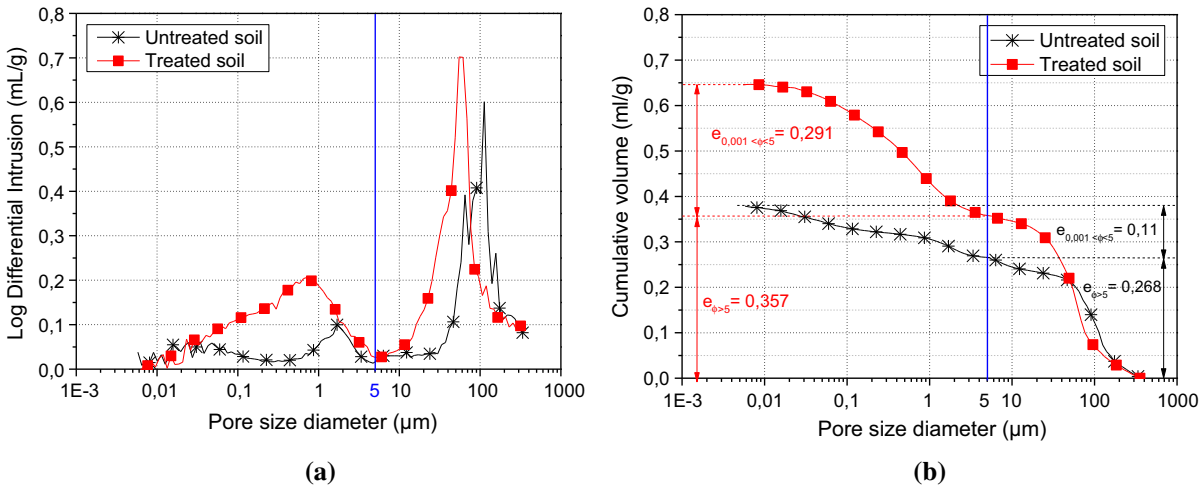

Fig. 31 Pore size distribution of untreated soil and treated soil with 1% CaO

Table 5 Calculation of the void indices of the two families

	ρ_d (t/m^3)	e_t	$e_{(0.0072\ \mu m < \phi \leq 5\ \mu m)}$	$e_{(\phi > 5\ \mu m)}$
Untreated soil	2	0.378	0.11	0.268
Treated soil	1.93	0.648	0.291	0.357

This increase of macro porosity after 24 h of treatment can be explained by the flocculation phenomenon and agglomeration of particles which occurs during the addition of the lime. Table 5 details the total void index measured from the mercury intrusion e_t, and the void index corresponding to the two pore families. After treatment, it is found that the quantity of the voids of the two families is greater than the ones in the untreated soil.

6 Conclusion

The study carried out aimed to study the effect of lime treatment on coarse soils in order to improve its erosion characteristics and be able to use it in embankment and hydraulic structures. The results of experimental study shown that the efficiency of treatment appears only after 24 h of curing. The increase of curing time until 3 months seems not to bring a subsequent change in the efficiency of lime treatment. This relatively quick stabilization seems to be related to the agglomeration of the fine particles. From the results of crumb test and unconfined compression test, this agglomeration remains maintained even under the effect of internal fluid flow. The results of the microstructure observation show an increase in the pore volume in general and more particularly in micro pore family. This phenomenon causes an increase in constrictions but the agglomeration of fine particles around the sand particles seems to prevent this departure and thus stabilize the soil against suffusion.

Acknowledgements These works were carried out in partnership with "Fédération Française des Travaux Publics - Comité Sol".

References

AFNOR (1992) NF P 11-300. Exécution des terassements: Classification des matériaux utilisables dans la construction des remblais et des couches de forme d'infracstructues routières. Recueil Normes Géotechniques, AFNOR

AFNOR (1993) NF P 98-230-3. Essais relatifs aux chaussées: Préparation des matériaux traités aux liants hydrauliques ou non traités—Partie 3: Fabrication en laboratoire de mélange de graves ou de sables pour la confection d'éprouvettes. Recueil Normes Géotechniques, AFNOR

AFNOR (1997) NF P 94-077. Sols: Reconnaissance et Essais—Essai de compression uniaxiale. Recueil Normes Géotechniques, AFNOR

Ahmed S, Lovell CW, Diamonds S (1974) Pores size and strength of compacted clay. J Geotech Eng 100(4):407–425

Al-Mukhtar M, Lasledj A, Alcover JF (2010) Behaviour and mineralogy changes in lime-treated expansive soil at 20°C. Appl Clay Sci 50(2):191–198

Al-Mukhtar M, Khattab S, Alcover JF (2012) Microstructure and geotechnical properties of lime-treated expansive clayey soil. Eng Geol 139–140:17–27

ANCOLD (1978) Bulletin of the Australian national committee on large dams, issue no. 51, p 55

ASTM standard D 6572-13 (2013) Standard test methods for determining dispersive characteristics of clayey soils by the crumb test. American Society for Testing and Materials

Basma AA, Tuncer ER (1991) Effect of lime on volume change and compressibility of expansive clays. Transp Res Rec 1295:52–61

Bell FG (1996) Lime stabilization of clay minerals and soils. Eng Geol 42:223–237

Boardman DI, Glendinning S, Rogers CDF (2001) Development of stabilization and solidification in lime–clay mixes. Geotechnique 51(6):533–543

Charles I, Herrier G, Chevalier C (2012) An experimental full-scale hydraulic earthen structure in lime treated soil. In: 6th International conference on scour and erosion, Paris, France, No. 290, p 8

Choquette M, Bérubé MA, Locat J (1987) Mineralogical and microtextural changes associated with lime stabilization of marine clays from eastern Canada. Appl Clay Sci 2:215–232

Cuisinier O, Auriol JC, Le Borgne T, Deneele D (2011) Microstructure and hydraulic conductivity of a compacted lime-treated soil. Eng Geol 123(3):187–193

Delage P, Pellerin FM (1984) Influence de la lyophilisation sur la structure d'une argile sensible du Québec. Clay Miner 19:151–160

Delage P, Marcial D, Cui Y-J, Ruiz X (2006) Ageing effects in a compacted bentonite: a microstructure approach. Geotechnique 56(5):291–304

Diamond S (1971) Microstructure and pore structure of compacted clays. Clays Clay Miner 19(4):239–241

Feia S, Dupla JC, Ghabezloo S, Sulem J, Canou J, Onaisi A, Lescanne H, Aubry E (2015) Experimental investigation of particle suspension injection and permeability impairment in porous media. Geomech Energy Environ 3:24–29

Haghighi I (2012) Caractérisation des phénomènes d'érosion et de dispersion des sols: développement d'essais et applications pratiques. Ph.D. thesis, Université Paris-Est

Howard AK, Bara JP (1978) Lime stabilization on Friant- Kern Canal. U.S. Bureau of Reclamation, Report No REC-ERC-76-20

Hunter D (1988) Lime induced heave in sulfate-bearing clay soils. J Geotech Eng ASCE 114(2):150–167

Khattab SAA (2002) Etude multi-échelles d'un sol argileux plastique traité à la chaux. Ph.D. thesis, University of Orléans, France

Lasledj A (2009) Traitement des sols argileux à la chaux: processus physico-chimique et propriétés géotechniques. Ph.D. thesis, University of Orléans, France

Le Runigo B (2008) Durabilité d'un limon traité à la chaux et soumis à différentes sollicitations hydrauliques: comportements physico-chimique, microstructural, hydraulique et mécanique. Ph.D. thesis, Université de Nantes

Le Runigo B, Ferber V, Cui YJ, Cuisinier O, Deneele D (2011) Performance of lime-treated silty soil under long-term hydraulic conditions. Eng Geol 118(1–2):20–28

Lemaire K, Deneele D, Bonnet S, Legret M (2013) Effects of lime and cement treatment on the physicochemical, microstructural and mechanical characteristics of a plastic silt. Eng Geol 166:255–261

Lioret A, Villar MV, Sánchez M, Gens A, Pintado X, Alonso EE (2003) Mechanical behaviour of heavily compacted bentonite under high suction changes. Geotechnique 53(1):27–40

Locat J, Tremblay H, Leroueil S (1996) Mechanical and hydraulic behaviour of a soft inorganic clay treated with lime. Can Geotech J 33(4):654–669

Makki-Szymkiewicz L, Hibouche A, Taibi S, Herrier G, Lesueur D, Fleureau JM (2015) Evolution of the properties of lime-treated silty soil in a small experimental embankment. Eng Geol 191:8–22

Maubec N (2010) Approche multi-échelle du traitement des sols à la chaux, études des interactions avec les argiles. Ph.D. thesis, Université de Nantes, France

Nguyen TTH (2015) Stabilisation des sols traités à la chaux et leur comportement au gel. Thèse de doctorat. Ecole doctorale Paris-Est

Osula DOA (1996) A comparative evaluation of cement and lime modification laterite. Eng Geol 42(1):71–81

Perry JP (1977) Lime treatment of dams constructed with dispersive clay soil. Trans ASAE 20:1093–1099

Petry TM, Berger EA (2006) Impact of moisture content on strength gain in lime-treated soils. In: Transportation Research Board, 85th Annual Meeting, Paper 06-2764 (p 16)

Rogers CDF, Glendinning S (1996) Modification of clay soils using lime. In: Rogers CDF, Glendinning S, Dixon N (eds) Lime stabilisation. Thomas Telford, London, pp 99–114

Rossi P, Ildefonse P, De Nobrega M, Chauvel A (1983) Study of structural and mineralogical transformations caused by compaction with or without lime addition to lateritic clays from Brazil. Bull Int Assoc Eng Geol 28:153–159

Stoltz G, Cuisinier O, Masrouri F (2012) Multi-scale analysis of the swelling and shrinkage of a lime-treated expansive clayey soil. Appl Clay Sci 61:44–51

Tran TD, Cui YJ, Tang AM, Audiguier M, Cojean R (2014) Effects of lime treatment on the microstructure and hydraulic conductivity of Héricourt clay. J Rock Mech Geotech Eng 6(5):399–404

Wild S, Arabi MR, Leng-Ward G (1993) Sulphate expansion of lime stabilized kaolinite II: reaction products and expansion. Clay Miner 28(4):569–583